15th IFK
Proc. of the 15th International Fluid Power Conference
<DOI>

Automation Framework for Constrained Optimal Trajectory Planning and Adaptive Robust Motion Control of Electrohydraulic Mobile Machines

Bobo Helian*, Christoph Keller, and Marcus Geimer

Institute of Mobile Machines (Mobima), Karlsruhe Institute of Technology (KIT), 76131 Karlsruhe, Germany

**Corresponding author: bobo.helian@kit.edu*

Abstract.

This study presents an integrated automation framework that unifies constrained optimal trajectory planning and adaptive robust motion control for electrohydraulic mobile machines. The proposed multi-layer architecture consists of command, planning, control, and actuation levels, ensuring seamless coordination between task execution and dynamic motion adaptation. A nonlinear filter-based time-optimal trajectory planner is developed to generate real-time feasible trajectories under kinematic and dynamic constraints, while an adaptive robust backstepping controller is designed to compensate for nonlinearities, parameter uncertainties, and external disturbances in hydraulic actuation. Additionally, a simplified control strategy is introduced for pressure-compensated systems to enhance industrial applicability. Comparative validation on an unmanned wheel loader demonstrates the proposed framework's effectiveness, achieving high tracking accuracy, strong robustness, and real-time constraint satisfaction. This work contributes to advancing autonomous and intelligent operation of electrohydraulic mobile machines by bridging planning and control in a cohesive system framework.

Keywords. Electrohydraulic systems, Constrained trajectory planning, Adaptive Robust Control, Mobile working machines, Automation control framework

1. INTRODUCTION

1.1 Motivation

The autonomy of mobile working machines [1], such as wheel loaders and excavators, has become a key research direction in both academia and industry. It aims to reduce dependency on skilled operators, improve operational safety, and enable continuous, autonomous operation in complex environments. Reliable automation of such machines fundamentally depends on two capabilities—trajectory planning that respects system constraints, and motion control that ensures precise and robust execution.

Electrohydraulic systems, though offering high power density, present major challenges due to nonlinearities, parameter uncertainties, and high-order hydraulic dynamics, which degrade tracking accuracy and robustness under varying loads and disturbances. Conventional linear controllers struggle to maintain performance in such conditions. Moreover, unlike electric drives, hydraulic systems are limited by flow saturation and slow responses due to fluid dynamics. Achieving time-optimal and constraint-satisfied trajectories while ensuring precise and robust execution remains a key challenge. These factors motivate the development of a unified control framework that integrates constrained trajectory planning with adaptive robust control for safe and effective autonomous operation of electrohydraulic mobile machines.

1.2 Related works

1) Trajectory planning strategies of hydraulic machines

Constraints pose a major challenge to achieving reliable motion control in mobile working machines, particularly in systems with multiple hydraulic actuators interacting with their environment. These constraints encompass both kinematic and dynamic aspects, such as input and hydraulic force limitations [2], and are influenced by factors including hydraulic configuration, safety requirements, and payload conditions specific to each machine [3]. Moreover, constraint boundaries may vary over time due to changes in operating conditions. Violating these constraints can cause actuator damage (e.g., cavitation), safety risks, and motion instability. Therefore, a robust and real-time constrained control strategy is crucial for enabling autonomous operation.

Various constrained control strategies have been proposed to address the limitations of electro-hydraulic systems. In [4], a motion tracking controller with full-state constraints was developed using a barrier Lyapunov function to ensure constraint satisfaction. The study [5] introduced an input-constrained control scheme that incorporates a bounded smooth hyperbolic tangent function to achieve asymptotic tracking. Furthermore, [6] presented a robust nonlinear control method for electro-hydraulic force systems considering output constraints. Although these works have advanced the understanding of constrained control in electro-hydraulic systems, most approaches focus on a single type of constraint and neglect the time-varying characteristics and interdependence among multiple constraints. Consequently, existing research still faces several open challenges: (1) Low-pass filters are often applied to handle aggressive reference inputs, but they introduce steady-state deviations, and the resulting trajectories are typically suboptimal—failing to reach the desired reference in minimum time while respecting the constraints. (2) The tracking accuracy of synthesized constrained trajectories is not guaranteed due to the nonlinearities and uncertainties inherent in electro-hydraulic systems, limiting the realization of optimal constrained motion control.

Integrating a precise motion tracking controller with real-time constrained trajectory planning provides a promising pathway to achieving both robust control performance and constraint satisfaction [3]. In [2] and [7], constrained adaptive robust motion tracking controllers were developed for linear motors and hydraulic actuators by combining a model-based motion controller with a nonlinear filter-type trajectory planner, yielding satisfactory results. The nonlinear filter planner, first proposed in [8], enables real-time generation of time-optimal trajectories that respect motion constraints. While [2] and [7] successfully demonstrated this approach in simple mechatronic systems, its application to complex electrohydraulic systems of mobile working machines remains largely unexplored. The trajectory planning of such machines introduces greater challenges due to multiple interacting constraints and strong coupling effects, motivating further development of advanced constrained trajectory planning strategies.

2) Precise motion control strategies of electrohydraulic actuators

While trajectory planners can generate optimal constrained trajectories for operations, tracking the desired trajectory may not be executed accurately. This is due to the nonlinear and uncertain nature of electro-hydraulic actuators [9], as well as external disturbances during mobile machine operation [10]. Therefore, a precise and robust motion control is essential for autonomous operation of mobile machines.

To achieve high-precision and robust control of electro-hydraulic systems, adaptive and nonlinear model-based strategies have been extensively explored [11]. Several methods have been proposed to handle uncertain disturbances and nonlinear effects. For instance, [10] developed an active disturbance rejection adaptive control scheme for hydraulic servo systems, while [12] proposed an H_∞-based control method with feedforward compensation to improve terrain disturbance rejection in mobile manipulators. To mitigate nonlinear friction, a modified LuGre model was introduced in [13], and a virtual decomposition control approach based on subsystem dynamics was presented in [14].

Among these approaches, Adaptive Robust Control (ARC) has shown outstanding potential in compensating uncertain loads, enhancing both accuracy and robustness [15]. As illustrated in Fig. 3, ARC integrates parameter adaptation with nonlinear feedback. Considering the high-order dynamics of hydraulic systems, an ARC backstepping scheme has been developed to ensure precise motion tracking under nonlinearities and uncertainties.ARC theory has been successfully extended to various electro-hydraulic configurations, such as electro-hydraulic actuators [9] and electro-variable pumps [16], and shows strong promise for multi-actuator mobile machines, where coupling dynamics remain an open challenge.

Furthermore, the integration and communication of these methodologies are essential for the robust and autonomous operation of mobile machines. However, such integrated approaches remain relatively underexplored, and further research is required to establish cohesive frameworks that seamlessly bridge planning and control for electro-hydraulic mobile machines [17].

1.3 Contributions

This study proposes a unified framework that integrates constrained trajectory planning and robust nonlinear motion control for autonomous operation of electrohydraulic mobile machines. An unmanned wheel loader is used as a representative case study, which is a highly automated unmanned system. The main contributions of this study are:

- A multi-level integrated control architecture is introduced, consisting of command-level: task command, mid-level: constrained trajectory generation, and lower-level: precise motion tracking. This structure ensures seamless coordination between planning and execution, contributing to robust control performance and flexible application.

- A time-optimal constrained trajectory planning algorithm is developed, utilizing a nonlinear filter-based planner with high-order of integrators, which explicitly considers both the kinematic structure and dynamic limitations of the wheel loader's electrohydraulic actuating system. This ensures feasibility and safety in real-world machines' automated operations.
- An Adaptive Robust Control (ARC) is designed for motion control of proportional valve-control hydraulic system, as the underlying controller. It effectively mitigates the impact of system nonlinearities and uncertainties by robust feedback and uncertain parameter online adaptation, ensuring accurate tracking of planned trajectories and overcoming limitations of traditional linear control methods.
- In addition to the advanced ARC method, a simplified controller was also designed, combining linear feedback with dynamic feedforward compensation. This lightweighted controller is specially designed for pressure-compensated hydraulic systems, offering a practical and easily implementable solution for industrial applications (e.g., wheel loads or excavators).
- The above proposed framework was validated on an unmanned wheel loader, a representative mobile machine with a standard electrohydraulic system and multiple actuators. Results demonstrate high trajectory-tracking accuracy and strong robustness against system uncertainties.

By bridging trajectory planning and adaptive robust control within a cohesive framework, the study offers a scalable and effective solution for future autonomous mobile machines.

2. CONTROL FRAMEWORK

The complete architecture integrates the above components into a hierarchical structure, as shown in Figure 2.1, explained as below:

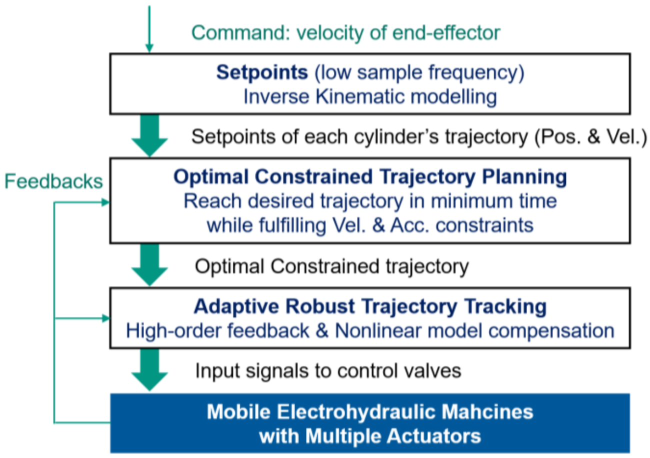

Figure 2.1. Control framework

1) **Command Layer:** The operator or task planner provides the desired end-effector motion (e.g., velocity), as command to the control system. The position & velocity of each actuator can be obtained in the form of discrete setpoints via inverse

kinematic model. This layer can be performed by autonomously or by operator remotely.

2) **Trajectory Planning Layer:** The trajectory planner generates an optimal constrained trajectory based on the setpoints. The planned trajectory reaches the desired setpoints in minimum time with high sampling frequency while simultaneously satisfying velocity and acceleration constraints.

3) **Motion Control Layer:** The motion tracking controller executes the planned trajectories with real time feedback and feedforward compensation. This controller design ensures robustness and precision despite the nonlinearities and uncertainties of the electrohydraulic system.

4) **Actuation Layer:** Control signals are transmitted to the hydraulic valves of the load arm actuators. The feedback from sensors of the electrohydraulic system is given to Trajectory Planning and Motion Control Layer in real-time.

This multi-layered structure ensures high adaptability. Feedback loops across multiple levels allow the system to dynamically compensate for disturbances and operational variations.

3. OPTIMAL CONSTRAINED TRAJECTORY PLANNING

Constraints of the motion control of the hydraulic actuator include the constraints of velocity (i.e., $\dot{x}^+$ and $\dot{x}^-$) and acceleration (i.e., $\ddot{x}^+$ and $\ddot{x}^-$), which are described in (3.1), while the stroke (position) bounds are static constraints that should be addressed at the task-planning level (i.e., setpoints in Figure 2.1) and not the focus of this section.

$$\begin{aligned} \dot{x}^- \leq \dot{x} \leq \dot{x}^+ \\ \ddot{x}^- \leq \ddot{x} \leq \ddot{x}^+ \end{aligned} \tag{3.1}$$

The assignments of the preset constraints for trajectory planning depend on the parameters and working conditions of the electro-hydraulic systems.

In this section, a two-integrator based nonlinear filter [8] is detailed to realize the online time-optimal trajectory planning to reach the desired reference while fulfilling the constraints on the velocity and acceleration (6). The two integrators chain is given by

$$\begin{bmatrix} x_p(i+1) \\ \dot{x}_p(i+1) \end{bmatrix} = \begin{bmatrix} 1 & T \\ 0 & 1 \end{bmatrix} \begin{bmatrix} x_p(i) \\ \dot{x}_p(i) \end{bmatrix} + \begin{bmatrix} \frac{T^2}{2} \\ T \end{bmatrix} \ddot{x}_p(i) \tag{3.2}$$

where T demotes the sampling time; i demotes the number of sampling periods. When $i = 0$, $\left[x_p(0), \dot{x}_p(0), \ddot{x}_p(0)\right]^T = [x_d(0), \dot{x}_d(0), \ddot{x}_d(0)]^T$. The state equation of the two integrators chain

$$\boldsymbol{x_p}(i+1) = \boldsymbol{A_c} x_p(\mathrm{i}) + \boldsymbol{B_c} \ddot{x}_p(i) \tag{3.3}$$

where $\boldsymbol{x_p}(\mathrm{i}) = \left[x_p(\mathrm{i}), \dot{x}_p(\mathrm{i})\right]^T$ is the system state when the time $t = i \times T$; $\ddot{x}_p$ here serves as the system input.

The error between the planned trajectory x_p and the originally expected command trajectory x_d is defined by $\boldsymbol{y}$, which is given as

$$\begin{aligned} y(i) &= x_p(i) - x_d(i) \\ \dot{y}(i) &= \dot{x}_p(i) - \dot{x}_d(i) \end{aligned} \tag{3.4}$$

where $\boldsymbol{x_d}$ is the given reference, indicating that when $y(i)$ tends to zero, $x_p(i)$ converges to $x_d(i)$. The error dynamics of the transformed system (10) is given by

$$\boldsymbol{y}(i+1) = \boldsymbol{A_c}\boldsymbol{y}(i) + \boldsymbol{B_c}v(i) \tag{3.5}$$

where $v(i) = \ddot{x}_p - \ddot{x}_d$.

In the error dynamics (3.4), the matrix $\boldsymbol{A_c}$ and $\boldsymbol{B_c}$ are both directly related to the sampling time T. To avoid the system error dynamics explicitly relying on the sampling time T, the following transformation is applied [11].

$$\boldsymbol{y}(i) = \boldsymbol{W}\boldsymbol{\eta}(i) \tag{3.6}$$

where

$$\boldsymbol{W} = \begin{bmatrix} T^2 & -\dfrac{T^2}{2} \\ 0 & T \end{bmatrix} \tag{3.7}$$

and $\boldsymbol{\eta}(i) = [\eta_1(i), \eta_2(i)]^T$. Matrix $\mathbf{W}$ is nonsingular, it implies that inverse transformation

$$\boldsymbol{\eta}(i) = \boldsymbol{W}^{-1}\boldsymbol{y}(i). \tag{3.8}$$

Combining the transformed formulation (3.8) and the error dynamics (3.5), it can be obtained that

$$\boldsymbol{\eta}(i+1) = \boldsymbol{A_d}\boldsymbol{\eta}(i) + \boldsymbol{B_d}v(i) \tag{3.9}$$

where

$$\boldsymbol{A_d} = \begin{bmatrix} 1 & 1 \\ 0 & 1 \end{bmatrix}, \ \boldsymbol{B_d} = \begin{bmatrix} 1 \\ 1 \end{bmatrix}. \tag{3.10}$$

In the above formulation (3.9), the system state $\mathbf{x_r}$ is transformed into an equivalent state $\boldsymbol{\eta}$. Since $\boldsymbol{W}$ is nonsingular, the eventual convergence to the origin of $\boldsymbol{\eta}$ implies the convergence of $\boldsymbol{y}$ to zero and the tracking of $\mathbf{x}_d$ is achieved.

To fulfil the requirements of the time-optimal trajectory planning objective and the given constraints (3.1), the control input of (3.9) is given by

$$v = \begin{cases} -\ddot{x}^{-}\mathrm{sat}\left(\dfrac{\delta}{\ddot{x}^{-}}\right), & \text{if } \delta \geq 0 \\ -\ddot{x}^{+}\mathrm{sat}\left(\dfrac{\delta}{\ddot{x}^{+}}\right), & \text{if } \delta < 0 \end{cases} \tag{3.11}$$

where $\mathrm{sat}(\bullet)$ is a saturation function; δ is obtained by,

$$\delta := \eta_2 + \frac{\gamma}{m} + \frac{m-1}{\alpha}. \tag{3.12}$$

The detailed design of γ, α, m, and further variables for constraints transformation are given in [7, 8], in which theoretical proof has been rigorously performed that the state point is forced to the origin of the sliding surface σ in minimum time, meanwhile, it also consequences on the fulfillment of the constraints on the velocity and acceleration.

As defined in (3.5) , the optimized acceleration of the trajectory can be written as

$$\ddot{x}_p = v + \ddot{x}_d \tag{3.13}$$

The optimized position x_p and velocity $\dot{x}_p$ can be calculated through differential equation (3.2). This optimized trajectory is given to motion controller in real time, which is detailed in the next chapter.

4. MOTION CONTROL

4.1. Adaptive Robust Controller Design

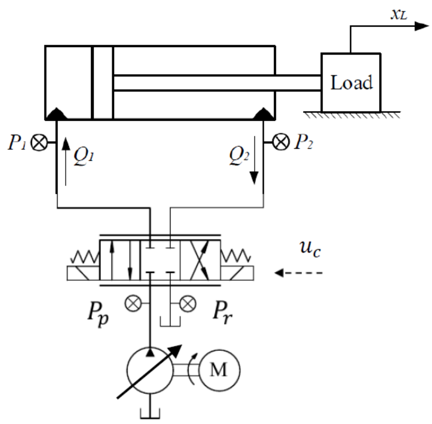

Figure 4.1 A simplified proportional valve-controlled cylinder

1) Dynamics modelling

A simplified general hydraulic system is presented in Figure 4.1, in which the motion of the hydraulic actuator is controlled by a proportional valve. The descriptions of symbols are listed in Table 1 in the Appendix. The dynamics of the cylinder motion can be modelled as

$$m\ddot{x}_L = P_1A_1 - P_2A_2 - b_v\dot{x}_L - b_c \cdot S_f(\dot{x}_L) + F_{\mathrm{d}}(x_L, \dot{x}_L, t) \tag{4.1}$$

where m represents the integrated mass of the inertia load; x_L represents the inertia load displacement; P_1 and P_2 represent the pressures of the head chamber and rod chamber; A_1 and A_2 represent areas of the two sides of the piston; b_v and b_c represent a viscous friction coefficient and a coulomb friction coefficient, respectively; $S_f(\bullet)$ represents a continuous function approximating the $\mathrm{sign}(\bullet)$. In addition, F_{d} represents a lumped uncertain nonlinearity, described as

$$F_{\mathrm{d}}(x_L, \dot{x}_L, t) = F_{\mathrm{dn}} + \tilde{F}_{\mathrm{d}} \tag{4.2}$$

where F_{dn} represents the nominal value of F_{d}.

The pressure dynamics of two chambers of the cylinder actuator can be modelled as

$$\begin{cases} \frac{V_1(x_L)}{\beta_e}\dot{P}_1 = -A_1\dot{x}_L - C_i(P_1 - P_2) + Q_1 \\ \frac{V_2(x_L)}{\beta_e}\dot{P}_2 = A_2\dot{x}_L + C_i(P_1 - P_2) - Q_2 \end{cases} \tag{4.3}$$

where C_i is the inner leakage coefficient. The flow rate linked to each chamber of the cylinder, controller by the proportional valve, can be modeled as

$$\begin{cases} Q_1 = k_{q1}\sqrt{|\Delta P_1|}\, u_c \\ Q_2 = k_{q2}\sqrt{|\Delta P_2|}\, u_c \end{cases} \tag{4.4}$$

where k_{q1} and k_{q2} are the throttling coefficients, $|\Delta P_i|$ (i=1,2) is the pressure drop due to throttling, and u_c denotes the effective valve control, which is proportional to the opening of valve spool.

The state-space variables of the pump control electro-hydraulic actuator are defined as $[x_1, x_2, x_3, x_4]^T = [x_L, \dot{x}_L, P_1, P_2]^T$. The uncertain parameters include m, b_v, b_c, β_e, C_i, and d_n. The uncertain parameter set is defined as $\theta = [\theta_1, \theta_2, \theta_3, \theta_4, \theta_5, \theta_6]^T$ in which $\theta_1 = 1/m,\ \theta_2 = b_v/m,\ \theta_3 = b_c/m,\ \theta_4 = F_{dn}/m,\ \theta_5 = \beta_e,\ \theta_6 = \beta_e C_i$.

The dynamics of the actuator motion control system can be parameterized as

$$\begin{aligned} \dot{x}_1 &= x_2 \\ \dot{x}_2 &= \theta_1(A_1x_3 - A_2x_4) - \theta_2x_2 - \theta_3S_f(x_2) + \theta_4 + \Delta \\ \dot{x}_3 &= \frac{1}{V_1(x_1)}(-\theta_5A_1x_2 - \theta_6(x_3 - x_4) + \theta_5g_1u_c) \\ \dot{x}_4 &= \frac{1}{V_2(x_1)}(\theta_5A_2x_2 + \theta_6(x_3 - x_4) + \theta_5g_2u_c) \end{aligned} \tag{4.5}$$

where $g_i = k_{qi}\sqrt{|\Delta P_i|},\ \Delta = \tilde{F}_{\mathrm{d}}/m$.

2) Controller design

This motion controller is a nonlinear model-based controller, based on an adaptive robust backstepping control structure, to accurately track the planned trajectory x_{p}. As shown in Figure 4.2, the controller includes two steps: motion tracking step and hydraulic force tracking step. Define $\hat{\theta}$ as the estimate of θ with $\hat{\theta}_{\min} < \hat{\theta} < \hat{\theta}_{\max}$ and $\tilde{\theta}$ as the estimation error, (i.e., $\tilde{\theta} = \hat{\theta} - \theta$).

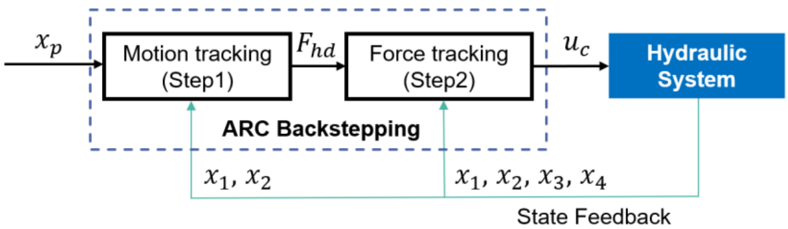

Figure 4.2 ARC Backstepping control strategy

The adaptation law is given by

$$\dot{\hat{\theta}} = \mathrm{Proj}_{\hat{\theta}}(\Gamma\tau) \tag{4.6}$$

where τ is an adaptation function introduced by Eq. (4.10) and (4.13); Γ is an adaptation rate matrix; $\mathrm{Proj}(\bullet)$ is a discontinuous projection [9].

Step 1: Motion tracking

The virtual control input F_h (i.e., hydraulic force) is designed to make the actuator position track the planned trajectory x_r. The output tracking error of the planned trajectory is defined as $z_1 = x_1 - x_r$. A switch function is then defined by

$$z_2 = \dot{z}_1 + k_1 z_1 = x_2 - x_{2eq},\ \ x_{2eq} = \dot{x}_r - k_1 z_1 \tag{4.7}$$

where $x_r(t)$ represents the planned trajectory to be tracked by output x_1 and k_1 is a positive feedback gain. It is straightforward to see that making z_1 converging to zero implies making z_2 converging to zero [31].

Considering the hydraulic force $F_h = P_1 A_1 - P_2 A_2$, the error dynamics is given by

$$\dot{z}_2 = \dot{x}_2 - \dot{x}_{2eq} = \theta_1 F_h - \theta_2 x_2 - \theta_3 S_f(x_2) + \theta_4 + \Delta - \dot{x}_{2eq}. \tag{4.8}$$

The desired hydraulic force F_{Ld} is defined as the control input of Step 1. Then, the ARC control input law is designed to minimize z_2, which is given by

$$\begin{aligned} &F_{hd}\left(x,\hat{\theta},t\right) = F_{hda} + F_{hds} \\ &F_{hda} = \frac{1}{\hat{\theta}_1}\left(\hat{\theta}_2 x_2 + \hat{\theta}_3 S_f(x_2) - \hat{\theta}_4 + \dot{x}_{2eq}\right) \\ &F_{hds} = F_{Lds1} + F_{Lds2},\ \ F_{hds1} = -\frac{1}{\theta_{1min}} k_2 z_2 \end{aligned} \tag{4.9}$$

where F_{hda} demotes an adaptive model compensation; F_{hds} demotes the robust feedback term; k_2 demotes a positive stabilizing feedback gain. Details on how to choose the nonlinear feedback (for F_{hds2}) are proposed in the literatures [15]. The adaptation function of Step 1 is given by

$$\tau_2 = \phi_2 z_2,\ \phi_2 = \left[F_{Lda}, -x_2, -S_f(x_2), 1,0,0\right]^T. \tag{4.10}$$

Step 2: Hydraulic force tracking

Control input u_c is synthesized to make the actual hydraulic force track the desired hydraulic force F_{Ld} (i.e., the input of Step 1). The input discrepancy of Step 1 is defined as $z_3 = F_h - F_{hd}$. The error dynamics is modelled as

$$\begin{aligned} \dot{z}_3 = &\ \dot{F}_h - \dot{F}_{hd} \\ = &\ u_c\theta_5\left(\frac{g_1 A_1}{V_1} + \frac{g_2 A_2}{V_2}\right) - \theta_5 x_2\left(-\frac{A_1^2}{V_1} - \frac{A_2^2}{V_2}\right) - \theta_6(x_3 - x_4)\left(-\frac{A_1}{V_1} - \frac{A_2}{V_2}\right) \\ &\ -\left(\dot{F}_{hdc} + \dot{F}_{hdu}\right) \end{aligned} \tag{4.11}$$

in which $\dot{F}_{hdc}$ and $\dot{F}_{hdu}$ represent the calculable part and uncalculable part of $\dot{F}_{Ld}$, respectively.

The ARC control law u_c, the valve control input, is given by

$$u_{\mathrm{c}}\left(x,\hat{\theta},t\right)=u_{\mathrm{ca}}+u_{\mathrm{cs}}$$
$$u_{\mathrm{ca}}=\frac{1}{\hat{\theta}_5\left(\frac{g_1A_1}{V_1}+\frac{g_2A_2}{V_2}\right)}\left(\theta_5x_2\left(-\frac{A_1^2}{V_1}-\frac{A_2^2}{V_2}\right)+\theta_6(x_3-x_4)\left(-\frac{A_1}{V_1}-\frac{A_2}{V_2}\right)+\dot{F}_{hdc}-\hat{\theta}_1z_2\right)$$
$$u_{\mathrm{cs}}=u_{\mathrm{cs1}}+u_{\mathrm{cs2}},\ \ u_{\mathrm{cs2}}=-\frac{1}{\hat{\theta}_{5\mathrm{min}}\left(\frac{g_1A_1}{V_1}+\frac{g_2A_2}{V_2}\right)}k_3z_3 \tag{4.12}$$

in which u_{ca} functions is an adaptive model compensation term; u_{cs} is the robust feedback term; k_3 is a positive stabilizing feedback gain; u_{cs2} is a nonlinear feedback term.

The adaptation function is given by

$$\tau=\tau_2+\phi_3z_3 \tag{4.13}$$

where ϕ_3 is defined as

$$\begin{aligned}\phi_3\ &=[z_2-\frac{\partial F_{Ld}}{\partial x_2}F_h,-\frac{\partial F_{hd}}{\partial x_2}x_2,-\frac{\partial F_{hd}}{\partial x_2}S_f(x_2),\frac{\partial F_{hd}}{\partial x_2},\\ &u_{\mathrm{ca}}\left(\frac{g_1A_1}{V_1}+\frac{g_2A_2}{V_2}\right)-x_2\left(-\frac{A_1^2}{V_1}-\frac{A_2^2}{V_2}\right),-(x_3-x_4)\left(-\frac{A_1}{V_1}-\frac{A_2}{V_2}\right)]^T.\end{aligned} \tag{4.14}$$

The theoretical proof of the two-step ARC backstepping controller has been rigorously performed in the literatures [9, 15] and it is omitted in this section. It is proved that the proposed controller guarantees the transient performance and asymptotical tracking in the presence of uncertainties only.

4.2. Lightweighted Controller Design for Pressure-Compensated Systems

In pressure-compensated hydraulic systems, the valve input can be represented as either the desired flow rate (for upstream compensation) or the desired actuator velocity (for downstream compensation). The pressure compensation mechanism effectively decouples the valve flow from load pressure variations, thereby simplifying the control design. As a result, a lightweight linear controller can achieve stable and accurate motion tracking in applications with moderate dynamic requirements.

$$v_{\mathrm{input}}=\dot{x}_p+k_{\mathrm{p}}(x_{\mathrm{d}}-x_1)+k_{\mathrm{v}}(\dot{x}_{\mathrm{d}}-x_2) \tag{4.15}$$

where k_{p} and k_{v} are positive feedback gains for position and velocity; the planed velocity $\dot{x}_p$ servers as the feedforward term for dynamic compensation. Thereby, the flow rate input can be calculated by

$$Q_{\mathrm{input}}=v_{\mathrm{input}}\boldsymbol{A} \tag{4.16}$$

where $\boldsymbol{A}$ denotes the effective piston area of the corresponding chamber (rod or head side), depending on the actuator's moving direction.

5. VERIFICATION ON UNMANNED WHELL LOADER

5.1. *System Formulation*

Figure 5.1. Two-wheel wheel loader by Quimo (picture from [18])

The machine used for a case study in this paper is an unmanned wheel loader, named two-wheel wheel loader, designed by Quimo as shown in Figure 5.1. The working arm of the wheel loader comprises three hydraulic cylinders, each named according to its function: the boom cylinder, arm cylinder, and tilt cylinder, as shown in Figure 5.2 (a). In addition, a counterweight cylinder is used to adjust the counterweight and ensure stability of the machine. All cylinders are equipped with linear position sensors, enabling the measurement of position and velocity. The hydraulic system adopts a load-sensing system with upstream pressure compensators. The valve block used in this study is an M4-12 load-sensing valve block coupled with an A10VO variable-displacement pump (both from Bosch Rexroth).

A co-simulation platform was developed in MATLAB/Simulink using the Simscape "Multibody" and "isothermal Fluid" library, integrating the multi-body dynamics of the wheel loader, the simplified upstream pressure-compensated hydraulic circuit, and their coupled dynamic interactions, as illustrated in Figure 5.2 (b). The density of the steel used for the working arm is set to 7800 kg/m³ in the simulation program.

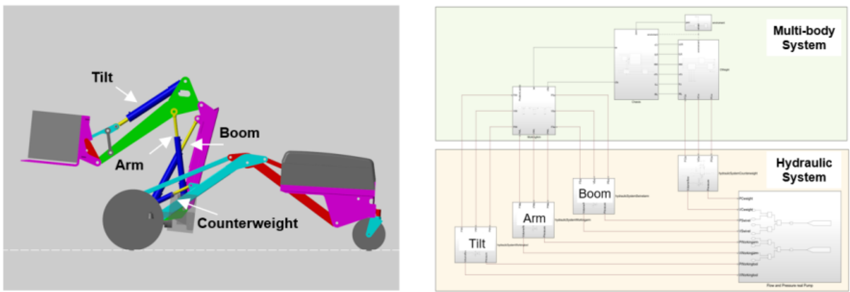

(a) Multi-body system (b) Co-simulation system

Figure 5.2. Simulation platform

5.2. *Single Cylinder Control Result*

Before machine-level verification, the proposed controller was first applied to a proportional valve–controlled single-cylinder system. Case 1 was conducted to validate the optimal constrained control performance of the planning strategy integrated with the proposed Adaptive Robust Controller (ARC) described in Section 4.1, referred to as C1. The maximum velocity limit $\dot{x}^+$ in Eq. (3.1) was set to 0.20 m/s for the planner, while the desired trajectory x_d had a maximum velocity of 0.23 m/s. As shown in Figure 5.3, controller C1 accurately tracked the planned constrained trajectory x_p that reached x_d at steady state while maintaining a smooth transient response. The velocity of the planned trajectory remained strictly within the prescribed constraint boundary throughout the motion, and the actual actuator velocity x_2 demonstrate the accurate tracking of the planned actuator velocity $\dot{x}_p$.

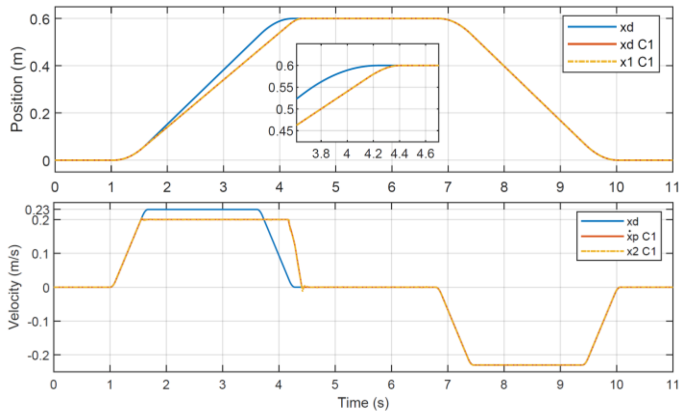

Figure 5.3. Positions and velocities in Case 1

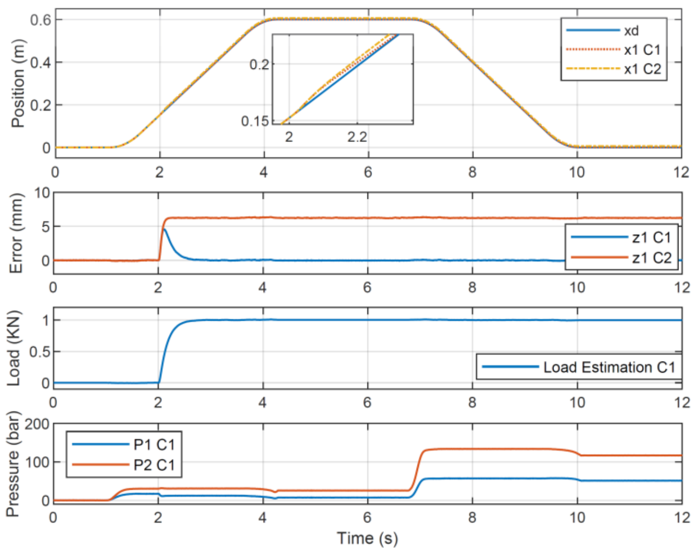

Figure 5.4. Position, tracking errors, load estimation in Case 2

Case 2 was performed to evaluate the anti-disturbance capability of the proposed controller. For comparison, another model-based controller with the same structure but without parameter adaptation was implemented as a baseline, denoted as C2. An external disturbance force of 1 kN was applied to the actuator at t = 2 s. As shown in Figure 5.4, both controllers experienced an immediate rise in tracking error following the disturbance. However, C1 rapidly suppressed the error and restored accurate tracking, demonstrating its superior disturbance rejection. This improvement is attributed to the effective online parameter adaptation in C1, which also provided accurate load estimation results, as shown in Figure 5.4. The pressure signals of both chambers of the hydraulic cylinder are also presented to provide additional insight into the internal force states of the actuator.

5.3. Working Arm Control Result

In this section, the proposed control framework (as illustrated in Figure 2.1) is fully applied to the working arm of the unmanned wheel loader, with an external mass load of 50 kg.

In this case, since the upstream pressure compensator defines the control input as the desired flow rate, the lightweight controller introduced in Section 4.2 is employed for the motion control layer. For comparison, a baseline controller (C3) is implemented—an open-loop controller with feedforward compensation but without feedback—to demonstrate the significance of closed-loop control in multi-actuator hydraulic systems.

Figure 5.5 shows the control results of the working arm, where the trajectories of all three cylinders are presented. The desired trajectories x_d are discrete setpoints generated at a low sampling frequency of 20 Hz. The proposed controller C1 generates real-time constrained trajectories x_p at 100 Hz, guiding the system smoothly toward x_d while optimally satisfying all constraints. The measured position signals x_1 demonstrate that all cylinders accurately track the planned trajectories under C1. In contrast, C3 exhibits poor tracking accuracy, with cumulative position deviations over time due to the absence of feedback control.

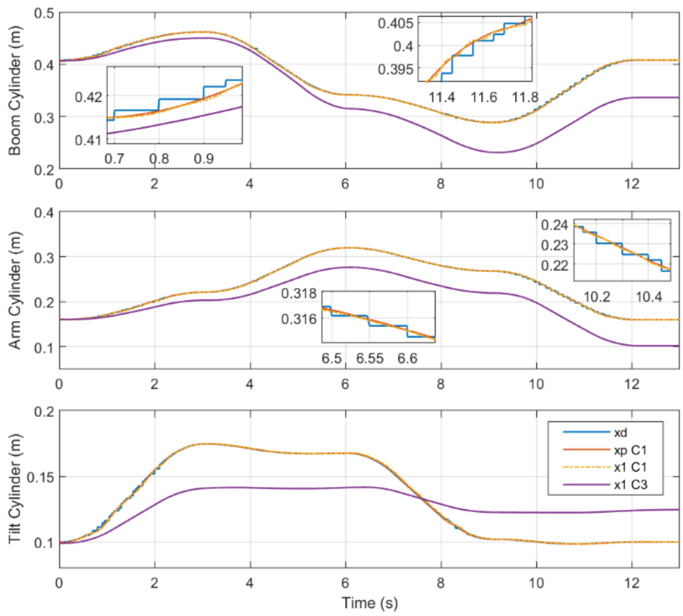

Figure 5.5. Results of working arm control

A comparison of C1 and C3 on the machine level is shown in Figure 5.6. The full operation cycle was designed to drive the end effector along a square trajectory in 12 seconds. Controller C1 maintained high tracking accuracy throughout both transient and steady-state phases, successfully accomplishing the desired motion. In contrast, C3 resulted in significant deviations at both the cylinder and end-effector levels. Demonstration videos corresponding to Figure 5.6 are provided in the **Appendix**.

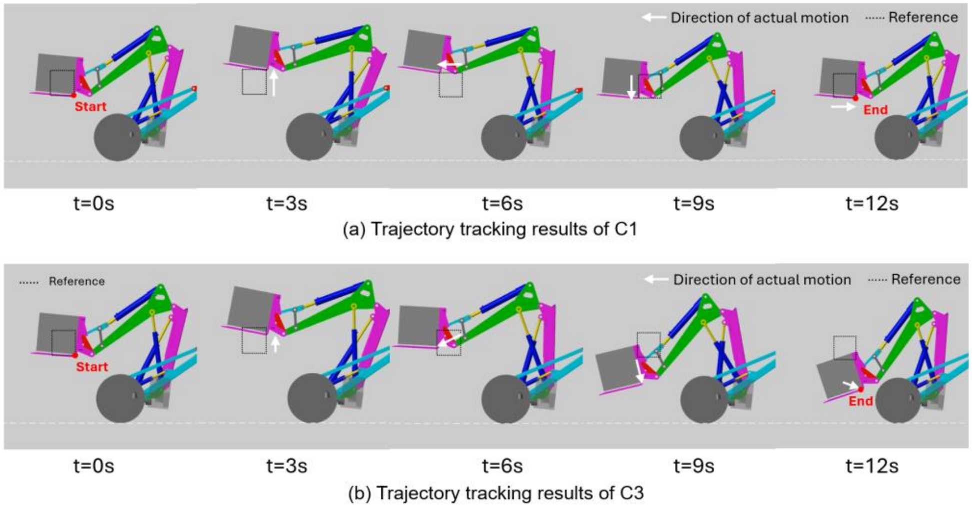

Figure 5.6. Comparative results shown on the machine

6. CONCLUSION AND FUTURE WORK

This paper presented a unified framework integrating constrained optimal trajectory planning and adaptive robust motion control for electrohydraulic mobile machines. The multi-layer architecture enables coordinated, constraint-satisfied, and robust motion execution. A nonlinear filter-based planner and an adaptive robust controller were combined to achieve precise, time-optimal tracking under nonlinearities and uncertainties. Experimental verification on an unmanned wheel loader demonstrated that the proposed approach outperformed baseline linear and open-loop controllers in tracking accuracy, robustness under uncertainty, and constraint compliance. A lightweight controller for pressure-compensated hydraulic systems was also introduced for practical industrial use. The proposed framework provides an effective and scalable basis for the autonomous operation of future electrohydraulic mobile machines.

In the future work, the integration of higher-level perception and task planning modules, such as environment sensing and adaptive task sequencing, will be explored to enable fully autonomous operation of mobile machines. Furthermore, future work will emphasize experimental validation across various types of machines under varying payloads and external disturbances. These extensions will further enhance the robustness, scalability, and industrial applicability of the proposed automation framework.

ACKNOWLEDGEMENT

This work was carried out as part of a research project funded by the Ministry of Economics, Labour and Tourism of Baden-Württemberg, Germany. Furthermore, we would like to thank the project partner QuiMo for designing the mechanical system of the unmanned wheel loader and providing its desired movement (i.e., Setpoints x_d in Section 5.3).

APPENDIX

The videos can be accessed via the link:
https://gitlab.kit.edu/bobo.helian/2RadLader_vedios.git .

7. REFERENCES

[1] M. Geimer, Mobile Working Machines, SAE International, Warrendale, PA, USA, 2020.

[2] B. Helian, Z. Chen, B. Yao, 'Constrained motion control of an electro-hydraulic actuator under multiple time-varying constraints', IEEE Trans. Ind. Inform., vol. 19, no. 12, pp. 11878–11888, 2023.

[3] A. Stentz, J. Bares, S. Singh, P. Rowe, 'A robotic excavator for autonomous truck loading', Auton. Robots, vol. 7, no. 2, pp. 175–186, 1999.

[4] Z. Xu, G. Qi, Q. Liu, J. Yao, 'ESO-based adaptive full-state constraint control of uncertain systems and its application to hydraulic servo systems', Mech. Syst. Signal Process., vol. 167, Art. no. 108560, 2022.

[5] Z. Lin, J. Yao, W. Deng, 'Input constraint control for hydraulic systems with asymptotic tracking', ISA Trans., vol. 129, pp. 616–627, 2022.

[6] W. Zang, Q. Zhang, J. Su, L. Feng, 'Robust nonlinear control scheme for electro-hydraulic force tracking with time-varying output constraint', Symmetry, vol. 13, no. 11, Art. no. 2074, 2021.

[7] M. Yuan, Z. Chen, B. Yao, X. Liu, 'Fast and accurate motion tracking of a linear motor system under kinematic and dynamic constraints: An integrated planning and control approach', IEEE Trans. Control Syst. Technol., vol. 29, no. 2, pp. 804–811, 2021.

[8] C. Guarino Lo Bianco, F. M. Wahl, 'A novel second-order filter for real-time trajectory scaling', Proc. IEEE Int. Conf. Robot. Autom. (ICRA), pp. 5813–5818, 2011.

[9] B. Helian, Z. Chen, B. Yao, et al., 'Accurate motion control of a direct-drive hydraulic system with an adaptive nonlinear pump-flow compensation', IEEE/ASME Trans. Mechatronics, vol. 26, no. 5, pp. 2593–2603, 2021.

[10] J. Yao, W. Deng, 'Active disturbance rejection adaptive control of hydraulic servo systems', IEEE Trans. Ind. Electron., vol. 64, no. 10, pp. 8023–8032, 2017.

[11] A. R. Plummer, N. D. Vaughan, 'Robust adaptive control for hydraulic servosystems', ASME J. Dyn. Syst., Meas., Control, vol. 118, no. 2, pp. 237–244, 1996.

[12] M. Rigotti-Thompson, M. Torres-Torriti, F. Auat Cheein, G. Troni, 'H∞-based terrain disturbance rejection for hydraulically actuated mobile manipulators with a non-rigid link', IEEE/ASME Trans. Mechatronics, vol. 25, no. 6, pp. 2686–2697, 2020.

[13] J. Yao, W. Deng, Z. Jiao, 'Adaptive control of hydraulic actuators with LuGre-model-based friction compensation', IEEE Trans. Ind. Electron., vol. 62, no. 10, pp. 6469–6477, 2015.

[14] J. Koivumäki, J. Mattila, 'Stability-guaranteed impedance control of hydraulic robotic manipulators', IEEE/ASME Trans. Mechatronics, vol. 22, no. 2, pp. 601–612, 2017.

[15] B. Yao, F. Bu, J. Reedy, G. T. C. Chiu, ‘Adaptive robust motion control of single-rod hydraulic actuators: Theory and experiments’, IEEE/ASME Trans. Mechatronics, vol. 5, no. 1, pp. 79–91, 2000.

[16] B. Helian, P. Mustalahti, J. Mattila, et al., ‘Adaptive robust pressure control of variable-displacement axial-piston pumps with a modified reduced-order dynamic model’, Mechatronics, vol. 87, Art. no. 102879, 2022.

[17] B. Helian, X. Liu, Z. Liu, M. Geimer, ‘Reinforcement learning-based autonomous control methodology of hydraulic excavators’, Proc. IEEE/RSJ Int. Conf. Intelligent Robots and Systems (IROS), pp. 4881–4888, 2025.

[18] Quimo GmbH, ‘Technical highlights’, https://www.quimo-gmbh.de/technology/, 2025.

Biographies

Bobo Helian received the Ph.D. degree in mechatronic engineering from Zhejiang University, Hangzhou, China, in 2021. Since 2021, he has been a Postdoctoral Researcher with the Institute of Mobile Machines (Mobima), Karlsruhe Institute of Technology (KIT), Karlsruhe, Germany. His research interests include advanced controls of electrohydraulic systems (e.g., EHA motion control, trajectory planning, constrained control, and adaptive robust control) and intelligent perception of mobile working machines (e.g., machine learning and computer vision).

Christoph Keller received the M. Sc. degree in mechanical engineering from the Karlsruhe Institute of Technology (KIT), Karlsruhe, Germany, in 2023. Since 2024, he has been a Ph.D. student with the institute of Mobile Machines (Mobima), KIT, Karlsruhe, Germany. His research interests include the simulation of mobile working machines (e.g. simulation with lumped parameters, co-simulation) and the product development of mobile working machines.

Marcus Geimer received the Diploma degree in mechanical engineering from the RWTH Aachen University, Aachen, Germany, in 1990, and the Ph.D. degree from the Institute of Hydraulics and Pneumatics, today named the Institute for Fluid Power Drives and Systems, RWTH Aachen University. Since 2005, he has been a Full Professor and the Director of the Institute of Mobile Machines (Mobima), Karlsruhe Institute of Technology (KIT), Karlsruhe, Germany. He started his industrial career in 1995 in the field of construction at the company Krupp Berco Bautechnik GmbH, Essen, Germany, where he was the Leader of the research group for hydraulic breakers. In 2000, he was with Bucher Hydraulics GmbH, Klettgau, Germany, where he led the construction and customer development for mobile hydraulics.